Liposomal clodronate inhibition of osteoclastogenesis and osteoinduction by submicrostructured beta-tricalcium phosphate.

Davison, NL; Gamblin, A-L; Layrolle, P; Yuan, H; de Bruijn, JD; Barrère-de Groot, F

Elsevier Editorial System(tm) for Biomaterials
Manuscript Draft

Manuscript Number:

Title: The immune response regulates osteoclastogenesis and osteoinduction by submicrostructured beta-tricalcium phosphate.

Article Type: FLA Original Research

Section/Category: Biomaterials and Regenerative Medicine (BRM)

Keywords: Osteoinduction, Calcium Phosphate, Osteoclasts, Foreign Body Response, Osteoimmunology, Surface microstructure

Corresponding Author: Mr. Noel Davison, M.S.E.

Corresponding Author's Institution: Xpand Biotechnology BV

First Author: Noel Davison, M.S.E.

Order of Authors: Noel Davison, M.S.E.; Anne Laure Gamblin; Pierre Layrolle; Huipin Yuan; Joost D de Bruijn; Florence Barrere-de Groot

Abstract: Bone graft substitutes such as calcium phosphates interact with the immune system through the foreign body response, which may bear important consequences for bone regeneration. We speculate that the unique surface microarchitecture of osteoinductive beta-tricalcium phosphate (TCP) stimulates the differentiation of invading monocyte/macrophages into osteoclasts, and that these cells may be essential to ectopic bone formation. To test this, porous TCP cubes with either submicron-scale surface architecture known to induce ectopic bone formation (TCPs, positive control) or micron-scale surface architecture (TCPb, non-osteoinductive negative control) were subcutaneously implanted on the backs of FVB strain mice for 12 weeks. Additional TCPs samples received local, weekly injections of liposome-encapsulated clodronate (TCPs+LipClod) to deplete invading phagocytes. TCPs induced osteoclast formation, evident by positive tartrate resistant acid phosphatase (TRAP) cytochemical staining and negative macrophage membrane marker F4/80 immunostaining. No TRAP positive cells were found in TCPb or TCPs+LipClod, only F4/80 positive macrophages and foreign body giant cells. TCPs stimulated subcutaneous bone formation in all implants, while no bone could be found in TCPb or TCPs+LipClod. In agreement, expression of bone and osteoclast gene markers was up-regulated in TCPs versus either TCPb or TCPs+LipClod, which were equivalent. In summary, submicron-scale surface structure of TCP induced osteoclastogenesis and ectopic bone formation in a process dependent on an unhindered immune response.

AUTHOR DECLARATION LETTER

We the undersigned declare that this manuscript is original, has not been published before and is not currently being considered for publication elsewhere.

We wish to draw the attention of the Editor to the following facts which may be considered as potential conflicts of interest to this work: N Davison, H Yuan, F Barrere-de Groot, and JD de Bruijn all work for Xpand Biotechnology, a privately held company located in the Netherlands who manufactures and sells calcium phosphates as bone graft substitutes world-wide. JD de Bruijn and H Yuan are also shareholders of Xpand Biotechnology and Progentix Orthobiology BV

We confirm that the manuscript has been read and approved by all named authors and that there are no other persons who satisfied the criteria for authorship but are not listed. We further confirm that the order of authors listed in the manuscript has been approved by all of us.

We confirm that we have given due consideration to the protection of intellectual property associated with this work and that there are no impediments to publication, including the timing of publication, with respect to intellectual property. In so doing we confirm that we have followed the regulations of our institutions concerning intellectual property.

We further confirm that any aspect of the work covered in this manuscript that has involved experimental animals has been conducted with the ethical approval of all relevant bodies and that such approvals are acknowledged within the manuscript.

We understand that the Corresponding Author is the sole contact for the Editorial process (including Editorial Manager and direct communications with the office). He/she is responsible for communicating with the other authors about progress, submissions of revisions and final approval of proofs. We confirm that we have provided a current, correct email address which is accessible by the Corresponding Author and which has been configured to accept email from biomaterials@online.be.

Signed by all authors as follows:

Noel Davison

Anne Laure Gamblin

Pierre Layrolle

Huipin Yuan

Joost D. de Bruijn

Florence Barrere-de Groot

The immune response regulates osteoclastogenesis and osteoinduction by submicrostructured beta-tricalcium phosphate.

Davison NL* [1,2], Gamblin AL[3], Layrolle P [3], Yuan H [1,2], de Bruijn JD [1,2,4], Barrere-de Groot F [2]

1 MIRA Institute, University of Twente, The Netherlands; 2 Xpand Biotechnology, The Netherlands; 3 INSERM UMR 957, University of Nantes, France; 4 Queen Mary University of London, United Kingdom

*Corresponding author: N.L.Davison@utwente.nl

Abstract: Bone graft substitutes such as calcium phosphates interact with the immune system through the foreign body response, which may bear important consequences for bone regeneration. We speculate that the unique surface microarchitecture of osteoinductive beta-tricalcium phosphate (TCP) stimulates the differentiation of invading monocyte/macrophages into osteoclasts, and that these cells may be essential to ectopic bone formation. To test this, porous TCP cubes with either submicron-scale surface architecture known to induce ectopic bone formation (TCPs, positive control) or micron-scale surface architecture (TCPb, non-osteoinductive negative control) were subcutaneously implanted on the backs of FVB strain mice for 12 weeks. Additional TCPs samples received local, weekly injections of liposome-encapsulated clodronate (TCPs+LipClod) to deplete invading phagocytes. TCPs induced osteoclast formation, evident by positive tartrate resistant acid phosphatase (TRAP) cytochemical staining and negative macrophage membrane marker F4/80 immunostaining. No TRAP positive cells were found in TCPb or TCPs+LipClod, only F4/80 positive macrophages and foreign body giant cells. TCPs stimulated subcutaneous bone formation in all implants, while no bone could be found in TCPb or TCPs+LipClod. In agreement, expression of bone and osteoclast gene markers was up-regulated in TCPs versus either TCPb or TCPs+LipClod, which were equivalent. In summary, submicron-scale surface structure of TCP induced osteoclastogenesis and ectopic bone formation in a process dependent on an unhindered immune response.

1. Introduction

The capacity of the immune system to regulate bone homeostasis, ranging from pathological disorders such as bone metastases to normal fracture healing, forms the focus of osteoimmunology, a term that was coined only in 2000 [1]. The immune system is also the key player in orchestrating the host reaction to implanted biomaterials, i.e. the foreign body response [2]. At a nexus between the two fields, it is intriguing to consider that specific interactions with the immune system may be essential for the functional performance of bone graft substitutes to even further stimulate bone tissue regeneration in bony defects.

Following the evolving insight into biomaterial design [3], particular emphasis has been devoted to understanding how physical properties of CaP may influence their bone forming performance. For instance, implant geometry [4], 3D surface concavities [5,6], and interconnected porous structure [7] have all been shown to promote bone formation. Most recently, material surface architecture on the submicron and micron scale has been shown to be particularly important to the osteoinductivity of a small, unique subset of CaP through an unknown biological mechanism [8,9]. It is at this CaP-tissue interface where proteins and ions are absorbed and exchanged, as a function of the material surface reactivity and physico-chemistry [10]. On a cellular level, it is at this interface where invading leukocytes interact with the material surface, mediating inflammation and tissue repair during the host response [11].

It has been speculated that in the case of osteoinductive CaP, invading tissue macrophages triggered by the host response may play a role in osteogenesis because of the dense and persistent presence of mononuclear cells surrounding an osteoinductive implant without fibrous tissue formation [12,13]. On the other hand, an adverse host response can also obstruct bone formation: in our previous work, chronic inflammation due to the addition of a polymeric carrier completely abrogated ectopic bone formation by osteoinductive beta-tricalcium phosphate (TCP) although the carrier dissolved relatively quickly [14]. Indeed, macrophages, the principal cell responsible for clearing a foreign body by phagocytosis, have been shown to express a distinct family of cytokines depending on their activation state in response to material properties such as surface chemistry, topography, and bioactivity [15,16].

Invading macrophages and other leukocytes secrete cytokines that can also spur the fusion and specialization of bone-resorbing osteoclasts from their monocyte/macrophage precursors. Pro-inflammatory cytokines such as TNF-α, IL-1, IL-6, IFN-gamma, and PGE2 activate T-cell expression of soluble RANKL (receptor activator of NF-κB ligand) the essential osteoclast differentiation factor, as well as up-regulate its membrane-bound receptor RANK on the surface of osteoclast precursors, thus inducing osteoclastogenesis [17–20]. On the other hand, other secreted cytokines such as IL-4 and IL-13 stimulate stromal cell expression of OPG (osteoprotegerin), the natural decoy receptor to RANKL, thus antagonizing osteoclast differentiation [21]. In this way, inflammation and osteoclastogenesis may be linked and dependent on the precise cytokine cascade and a biomaterial substrate supporting pre-osteoclast fusion and differentiation. Osteoclasts have also been implicated with the functionality of osteoinductive CaP with reports that osteoclasts form prior to ectopic bone formation [22] and that their inhibition may stunt osteoinduction [23,24].

Interestingly, macrophage-mediated inflammation has been associated with pathological heterotopic ossification (HO) that results in marrow-containing bone neogenesis in the muscle tissue triggered by injury. However, when liposome-encapsulated bisphosphonate was locally administered to selectively deplete tissue macrophages in a transgenic mouse model of HO, osteogenesis was significantly blocked. This effect was attributed to the elimination of macrophage-secreted BMP4 at the injury site [25]. In an experimental mouse model of osteoarthritis, macrophage depletion, again by liposomal bisphosphonate, resulted in the reduction of osteophyte formation – heterotopic bone nodules in the synovium – attributed to reduced macrophage expression of osteogenic TGFβ, BMP2, and BMP4. And as it pertains to the natural regenerative capacity of bone, when macrophages were depleted using liposomal clodronate in a long bone fracture model, bone formation in the fracture callus was fully inhibited [26], shown elsewhere to be likely mediated by macrophage-expressed TNF-α and IL-6 [27]. These studies and others like them emphasize the apparent importance of macrophages and phagocyte relatives to both aberrant and reparative bone formation.

Importantly, both bone and immune cells have been shown to be highly sensitive to surface microstructure of CaP. In our previous research investigating two TCP ceramics with different sized surface features, both ectopic bone formation and the presence of actively resorbing osteoclast-like multinucleated cells were strongly promoted on *submicron-scale* TCP surface features (submitted article). On the other hand, no ectopic bone and scarce non-resorbing multinucleated cells were found on the TCP implants with *micron-scale* surface features. Following on these findings, we asked whether these multinucleated cells were differentiated osteoclasts or merely fused macrophages, i.e. foreign body giant cells, and whether they play a role in the resulting ectopic bone formation by forming and functioning differently on the two different topographies.

In order to investigate these questions, we implanted the same two TCP ceramics with equivalent chemistry but different surface microstructure – serving as positive and negative controls – in a recently validated mouse model of subcutaneous osteoinduction [28] and analyzed the ectopic bone formation and the phenotype of formed multinucleated cells using (immuno-)histological and gene expression analysis. To address the role that these multinucleated cells play in osteoinduction, we applied liposome-encapsulated clodronate (LipClod) to disrupt the host immune response and selectively deplete invading phagocytic mononucleated precursor monocyte/macrophages [29] and then evaluated ectopic bone formation.

2. Materials and Methods

2.1 Preparation and Characterization of Porous TCP Cubes

TCP powders were synthesized as previously described [14]. Briefly, calcium hydroxide and phosphoric acid (both from Fluka) were mixed at a Ca/P ratio of 1.50. TCP powders with small (TCPs) or big grains (TCPb) in the final ceramics were prepared by controlling the reaction rates. The powders were foamed with diluted H_2O_2 (1%) (Merck) at 60°C then dried at room temperature to get porous green bodies. The dry green bodies were subsequently sintered at 1050°C or 1100°C for 8 hours to achieve small and big grains for TCPs and TCPb, all respectively.

Porous cubes (4 x 4 x 4 mm) were machined from the ceramic bodies using a wet saw and then ultrasonically cleaned in successive baths of acetone, ethanol, and distilled water, and dried. Prior to implantation, TCP cubes were heat sterilized at 160°C for 2 hours. Crystal chemistry of the materials was analyzed by X-ray diffraction (Rigaku Miniflex II) scanning the range $2\theta = 25–45°$ (step size = 0.01°, rate = $1° \min^{-1}$) and confirmed to be beta-TCP as previously described [14].

The TCP ceramics were characterized to confirm that they were composed of different microstructure but similar macrostructure as previously reported (article submitted). Surface microstructure was characterized by scanning electron microscopy (SEM) (JEOL JSM-5600) after sputter coating with gold for 90 s (JEOL JFC 1300) and > 50 surface grains and micropores were measured in the using Image J image analysis software (NIH, USA). To measure the surface profile (i.e., surface roughness), SEM stereo-micrographs of the same location taken at two different tilt angles (2500x, ±5°) were digitally reconstructed into three-dimensional surfaces for automated profile analysis using MeX v5.1 software (Alicona Imaging, Austria). Additionally, porosity and total pore area were determined by mercury intrusion testing (Table 1) (Micromeritics, USA).

In summary, the synthesis of TCPs and TCPb resulted in submicron-scale and micron-scale surface grains, micropores, and roughness, respectively. The ceramics possessed similar total porosity but different total pore area owing to the smaller surface features of TCPs.

2.2 Subcutaneous implantation in FVB mice

Ethical approval for animal experimentation was obtained from the local ethical committee (CREEA). The animals were housed in certified premises at the Experimental Therapeutic Unit at the Faculty of Medicine, University of Nantes, France. Animals were stabled in cages with food and water *ad libidum* with artificial day/night cycle of 12 h and regulated temperature of 20 ± 1°C.

Five-week-old male FVB strain mice (n = 14) were received from Charles River Laboratory (France) and allowed to equilibrate to their new surroundings for one week. Prior to surgery, the mice were placed under general anesthesia using isoflurane gas (2.5 % in air, 2.5 l/min, Forene). Analgesic (Buprenorphine 60 µl/kg, Buprécare, MedVet) was subcutaneously injected at the time of surgery and 1 day later. Backs of animals were shaved and disinfected with iodine solution and sterile gauzes and covered with a surgical sheet. Subcutaneous dorsal pockets were created using a scalpel and blunt nosed forceps and one TCP cube was inserted per pocket. Skin incisions were tightly closed with degradable sutures (Vicryl 4-0, Ethicon). Immediately following surgery, sterile liposomal clodronate (100 µl) (Clodronate Liposomes Foundation, The Netherlands) was injected into one pocket containing TCPs per animal. The same volume of sterile saline was injected into one pocket containing TCPs and one containing TCPb per animal, serving as positive and negative controls, respectively. This same injection regiment was repeated once a week and then animals were sacrificed after 12 weeks by inhalation of an overdose of carbon dioxide gas.

At this time, one long incision through the skin was made down the back and carefully separated from the muscle using a scalpel. TCP implants were carefully cut away from the soft tissue and skin and placed in vials containing either 4% formaldehyde for histological analysis or in RNAse/DNAse free tubes containing 1 mL TRI® Reagent (Sigma-Aldrich) for RNA isolation and qPCR. Histological replicates were stored at 4°C for and qPCR replicates were frozen at -80°C for further processing.

2.3 Histological Processing and imaging

TCP explants from 9 mice were processed for histological analysis. Explants were placed in cassettes and then decalcified in 4.13% EDTA/0.2% paraformaldehyde in PBS (pH 7.4) at 50°C using an automated microwave decalcifying apparatus (KOS Histostation, Milestone Med. Corp. MI, U.S.A). Samples were periodically checked with x-ray to ensure complete and consistent decalcification, which required up to 17 days. After complete decalcification, samples were then rinsed with tap water and dehydrated in ascending series of ethanol baths: 80, 95, 100%, and finally in butanol for 30 min (Automated dehydration station, Microm Microtech, France). Samples were then impregnated in liquid paraffin at 56°C (Histowax) and embedded at -16°C. Embedded explants were completely sectioned at 4-7 locations spaced ~500 μm using a standard microtome (Leica RM2250) set at 5 um thickness. Following the various stains described below, coverslips were mounted with Pertex and slides were digitally scanned at up to 40x magnification (NanoZoomer 2.0RS, Hamamatsu Corp. Japan) and analyzed with virtual microscope software (NDP View, Hamamatsu Corp).

2.4 Masson's Trichrome Staining for Bone Formation

Sections were stained by Masson's trichrome technique by using an automated coloration station (Microm, Microtech). This staining combined hematoxylin for cell nuclei in blue/black, fuchsin for cytoplasm, muscle and erythrocytes in red, and bright green for collagen and allowed the visualization general tissue response and new bone formation. Cover slips were mounted with Pertex and digitally scanned as previously described. The presence of bone in each histological sample was carefully analyzed by multiple researchers in at least 5 different sections taken at different levels throughout the explant.

2.5 Immunohistochemical Staining of Macrophage Marker F4/80 and Osteoblast Transcription Factor Osterix

Immunohistochemical staining of murine macrophage membrane marker F4/80 and osteoblast transcription factor Osterix served to identify macrophages and osteoblasts in serial histological sections. Sections were first deparrafinized in Ottix histological solvent (3 x 5 min), rehydrated in a graded ethanol series (100%, 3 x 5 min; 95%, 1 x 5 min; 80%, 1 x 5 min), and then rinsed in distilled water (3 x 5 min). To retrieve antigens, sections were incubated in citrate buffer, pH 6, at 95°C for 10 min. Sections were then incubated with 3% H_2O_2 for 15 min to inactivate endogenous peroxidase, rinsed with TBS-Tween 0.05% pH 7.6, blocked with 5% normal goat serum in 1% BSA in TBS-0.05% Tween pH 7.6 at room temperature for 30 min, then incubated at 4°C overnight with primary antibodies (AbCAM) targeting F4/80 (rabbit anti-mouse monoclonal, 1:100) and sp7/Osterix (rabbit polyclonal, 1:800) diluted in blocking buffer. Sections were again rinsed with TBS-Tween then incubated with secondary goat anti-rabbit antibody (Dako) diluted 1:200 in blocking buffer for 30 min at RT, rinsed with TBS-tween, incubated with streptavidin-linked HRP (Dako) for 30 min at RT, and finally visualized with DAB chromogen (Dako) with Mayer's hematoxylin counterstain. Cover slips were mounted with Pertex and digitally scanned as previously described.

2.6 Cytochemical Staining of Osteoclast Enzyme Marker TRAP

Cytochemical staining of osteoclast enzyme tartrate resistant acid phosphatase (TRAP) was used as a marker to identify osteoclasts in histological sections. TRAP staining was performed using a commercial staining kit (Acid Phosphatase Leukocyte Staining Kit, Sigma) following the manufacturer's instructions. Briefly, staining solution was prepared with Fast Red TR salt (3.9 mM), naphthol AS-TR phosphate disodium salt (2.3 mM), N-N dimethylformamide (68 μM), and L(+)-tartaric acid (100 mM) all diluted in sodium acetate buffer (0.1 M, pH 5.2). Deparaffinized sections were incubated in the solution for 90 min at 37°C and then counterstained with Mayer's hematoxylin. TRAP positive stained cells appeared red.

2.7 Gene expression by qPCR

The gene expression of replicate TCP explants from 5 mice was analyzed by qPCR. Frozen samples were thawed and thoroughly pulverized in TRI® Reagent (Sigma-Aldrich) using a motorized pestle homogenizer. Samples were centrifuged to remove TCP particles, and the RNA in the supernatant was precipitated in chloroform following the manufacturer's instructions. Total RNA concentration and purity was measured using a Nanodrop machine. Reverse transcription of cDNA was performed using a ThermoScript First-Strand kit (Invitrogen).

Quantitative PCR (qPCR) was performed on a BioRad CFX 96 System. The PCR reactions were performed with 20 ng cDNA in a total volume of 10 µL containing iQ SYBR Green Supermix (Biorad) and forward and reverse primers (300 nM). After an initial activation step for 30 seconds at 98°C, 40 cycles were run of a two-step PCR consisting of a denaturation step at 95°C for 15 seconds and annealing and extension step at 60°C for 30 seconds. Subsequently the PCR products were subjected to melting curve analysis to test if any unspecific PCR products were generated.

qPCR primers were designed using Primer-BLAST (www.ncbi.nim.nih.gov) spanning at least 1 intron to avoid amplification of genomic DNA (Table 3). Expression of housekeeping genes HPRT and cyc1 was not affected by the experimental conditions and were thus used for endogenous normalization of the gene targets. Relative fold expression of the normalized gene targets was calculated versus expression levels in the negative control, TCPb.

2.8 Statistics

Statistical comparisons of gene target expression were performed using One-way ANOVA and Tukey's post hoc tests in GraphPad Prism 6.0 software. P values < 0.05 were considered significant.

3 Results

3.1 Ectopic bone formation and tissue response

TCPs and TCPb porous cubes were implanted in subcutaneous pockets on the backs of mice and resulting ectopic bone formation was evaluated both by histological and whole-sample gene expression analysis. During implantation some replicates intended for histological analysis were lost due to incomplete wound healing, particularly for TCPs receiving LipClod treatment. After careful scrutiny of multiple random levels of each harvested sample, ectopic bone tissue could be identified in all of the TCPs explants (7 out of 7) and in none of the TCPb explants (0 out of 8), thus validating these materials as positive and negative controls in this model of osteoinduction. Importantly, no bone was found in TCPs implants treated locally with LipClod (0 out of 5) to deplete the invading phagocytes (Table 4).

In TCPs, bone formation was little in amount compared to the total implant area; however, cuboidal osteoblasts, osteocytes in characteristic lacunae, and multinucleated osteoclast-like cells could all be identified. Moreover, a difference in the tissue response was observed in that the pore structure of TCPs was generally occupied by darkly stained highly condensed collagen fibrils whereas that of TCPb appeared to be lighter stained loose connective tissue. In TCPs samples treated with LipClod, sparse connective tissue in the pore structure appeared disorganized and did not stain the same dark, vivid green as the dense collagen observed in TCPs control (Figure 1).

Expression of mature bone markers BSP and OCL was significantly up-regulated in TCPs versus the negative control TCPb (~220 fold, P = 0.039; 3 fold, P = 0.0002; respectively); however, expression levels in TCPs treated with LipClod were unchanged versus TCPb (P = 0.930 and 0.999, respectively), substantiating the histological analysis that LipClod treatment blocked bone formation by TCPs (Figure 1).

3.2 Identification of TRAP positive, F4/80 negative osteoclasts on TCP

Enzymatic staining for osteoclast marker TRAP served to identify osteoclasts in the implants. Because mature osteoclasts are F4/80 negative [30–32], we compared TRAP and F4/80 staining of the same multinucleated cells in serial sections in order to unambiguously differentiate between multinucleated osteoclasts and fused macrophage foreign body giant cells.

In TCPs, TRAP positive giant cells were located primarily between stretches of ectopic bone attached to the material surface. In serial sections, these same cells were confirmed to be F4/80 negative, establishing their identity as differentiated osteoclasts rather than fused macrophages. Not all TRAP positive osteoclasts were located next to bone suggesting that the presence of bone may not be necessary for their formation. Moreover, not all multinucleated cells in TCPs were TRAP positive indicating the heterogeneity of multinucleated cells throughout the explant. In contrast, TRAP positive cells – either mononucleated or multinucleated – could not be found in neither TCPb nor in TCPs treated with LipClod. The multinucleated cells colonizing these implants were uniformly F4/80 positive.

In support of the finding that TCPs promoted osteoclastogenesis while TCPb did not, osteoclast gene markers TRAP, calcitonin receptor, and osteoclast transcription factor NFATc1 were analyzed and indeed, these markers were significantly up-regulated in TCPs (fold differences = 2, 234, and 1; P = 0.011, 0.021, and 0.046, all respectively). In contrast, LipClod treatment left them unchanged versus TCPb (P = 0.564, 0.999, and 0.351, respectively). In an effort to explain these results, expression of the critical osteoclast-signaling axis RANK-RANKL-OPG was analyzed, showing that RANK expression was sharply down-regulated in TCPs + LipClod versus TCPs control (1.6 fold, P = 0.009), probably due to the selective eradication of phagocytic monocyte/macrophage osteoclast precursors. The expression of RANKL and OPG were also lower in TCPs after treatment with LipClod than without (0.9 and 1.1 fold difference, respectively), although these differences were not significant (P = 0.152 and 0.105, respectively). Thus, the reason for osteoclast depletion may have been more due to loss of RANK-expressing monocyte/macrophage osteoclast precursors rather than alteration of the balance between RANKL and its decoy antagonist OPG.

3.3 Macrophage colonization and depletion

Macrophage-specific membrane marker F4/80 was visualized using immunohistochemistry in order to evaluate the efficacy of LipClod treatment in depleting phagocytic macrophages and foreign body giant cells characteristic of the foreign body reaction. Indeed, LipClod treatment effectively depleted F4/80 positive cells particularly at the outer surfaces of the implant accompanied by large numbers of negatively stained mononuclear cells and cell fragments indicative of LipClod-initiated apoptosis. In contrast, the outer edge of TCPs control was prominently lined with a dense layer of F4/80 positive macrophages.

Despite the clear efficacy of macrophage depletion at the edge of the TCPs implants, positively stained macrophages were still present in the inner pore structure, similar to the untreated TCPs control. There in particular, F4/80 positive multinucleated cells colonized the surface of TCPs regardless of LipClod treatment.

Positively stained macrophages were also present in TCPb, but appeared substantially less organized than TCPs control. In particular, F4/80 positive macrophages did not densely line the outer edge of TCPb as on TCPs control. In the pore structure, however, F4/80 positive multinucleated cells were observed similar to TCPs with and without LipClod treatment.

In support of these histological results, F4/80 gene expression was lower with LipClod treatment versus TCPs control (0.7 fold difference), though not significantly different ($P = 0.144$) confirming that F4/80 positive macrophage depletion was incomplete. F4/80 expression was equivalent between TCPs and TCPb controls (0.2 fold difference), despite differences in staining intensity and organization.

3.4 Osteoblast differentiation inhibited by phagocyte depletion

To evaluate if LipClod treatment affected osteoblast differentiation associated with osteoinduction by TCPs, immunohistochemical staining of Osterix confirmed the presence of osteoblast-like cells in TCPs treated with LipClod, though less frequent than in TCPs without treatment. Moreover, whereas Osterix positive cuboidal osteoblasts were mainly located on or next to ectopic bone in the TCPs control, they were located in loose connective tissue contained in the pore structure of TCPs + LipClod. No Osterix positive cells were evident in TCPb (not shown). These histological results were substantiated by significantly lower expression of osteoblast transcription factor Runx2 versus TCPs (2 fold, $P = 0.028$) and equivalent expression to TCPb ($P = 0.726$). Versus TCPb, Runx2 expression in the TCPs control was also higher, trending on statistical significance (1.5 fold, $P = 0.062$).

4 DISCUSSION

By identifying multinucleated cells that were positively stained for osteoclastic enzyme TRAP but negatively stained for macrophage membrane marker F4/80 and vice versa, the distinct presence of both OCl and FBGC were found on the surface of osteoinductive submicrostructured TCPs in subcutaneous implants. Although FBGC widely populated the surface of non-osteoinductive microstructured TCPb, no such TRAP positive multinucleated cells could be found. Osteoclast markers were significantly down-regulated on TCPb, suggesting that osteoclastogenesis is not common to all CaP but is preferentially directed by osteoinductive surface microstructure. This finding could provide an explanation for the widely varied and conflicting reports on the identity of multinucleated cells surrounding different CaP in various implantation models [33–36]: all CaP are not created equal; one material with a particular surface architecture may promote osteoclastogenesis while another composed of the same chemistry and macrostructure may not. In support of this finding, our previous work (article submitted) demonstrated that TCPs promotes the formation and resorptive activity of OCl in vitro, emphasizing the directive role of surface submicron surface structure on osteoclastogenesis. It is interesting to consider that while biomaterials comprising a wide range of material chemistries and structures trigger FBGC formation during the foreign body response [2], an osteoinductive CaP material directs the formation of the three major bone cells in a heterotopic location: OCl (multinucleated, F4/80 negative, TRAP positive, residing on the material surface; Figure 2), osteoblasts (cuboidal, strongly Osterix positive, residing on the bone surface; Figure 4), and osteocytes (weakly Osterix positive, residing in bone lacunae; Figure 4).

In addition to this result, LipClod treatment impeded both bone formation and osteoclastogenesis, substantiated by equivalent bone and osteoclast markers to the negative non-osteoinductive control. Our hypothesis that the host response to osteoinductive TCP may determine ectopic bone formation is therefore confirmed. LipClod treatment was shown to potently deplete F4/80 positive macrophages around the perimeter of the implants as intended; however, F4/80 positive mono- and multinucleated cells could still be found in the internal pore structure of the implants. Moreover, F4/80 gene expression was not significantly down-regulated compared to non-treated controls. Together, these results suggest that although LipClod treatment successfully depleted invading macrophages at the implants' outer surface, the liposomes were unable to substantially penetrate the inner pore structure thereby allowing macrophages migrating from the internal vasculature to survive and proliferate. Nonetheless, LipClod treatment evidently disrupted the normal phagocyte response enough to prevent bone and OCl formation.

LipClod is extensively used in the literature to study the role of macrophages in various disorders where inflammation and wound healing play a key role. The function and efficacy of LipClod depletion of phagocytes, particularly macrophages, has been thoroughly researched for over 20 years and is a strategy that has been used in more than 800 peer reviewed citations, attesting to its wide breadth of applications as a research tool [37]. Mechanistically, when a clodronate-encapsulated liposome is phagocytosed, the liposome is opened by intracellular lysozyme and the drug is released in the cytoplasm where it is metabolized into a toxic ATP analog resulting in both apoptosis and necrosis [38,39]. The specificity of LipClod in its ability to deplete only "professional" phagocytes arises from the liposomes' fast clearance time, the short half-life, non-toxicity of free clodronate, and the inability of the liposomes to passively infiltrate the cell membrane [29].

Expounding on the hypothesis that the host response to an osteoinductive implant determines its osteogenic capacity, we speculated that the lack of multinucleated cells such as OCl and FBGC would impede ectopic bone formation. This was further supported by our previous observations in which the presence and resorptive activity of these cells on implanted TCP was correlated with osteoinductivity. LipClod treatment was selected to deplete these cells because it targets their mutual monocyte/macrophage phagocyte precursors as well as OCl themselves. Although FBGC were still present in the internal pore structure of the treated implants, no TRAP positive multinucleated cells could be found in the treatment samples and OCl gene markers were significantly down-regulated, suggesting that osteoclastogenesis or osteoclast survival was reduced. It is unclear if OCl simply were unable to differentiate due to depleted levels monocyte-macrophage precursors or whether OCl formed but then were directly depleted in the same mechanism as macrophages – through phagocytosis of LipClod – as reported in the literature [40,41]. A time course study might be useful in illuminating this question. In either case, ectopic bone formation was impeded in the absence of depleted TRAP positive OCl, although F4/80 positive mononuclear and multinucleated MP were still present.

The question remains how phagocytes such as OCl or MP mediate ectopic bone formation. Previous results from our group showed that when OCl and to a lesser extent MP are cultured on osteoinductive TCP, they secrete soluble factors that potently induce alkaline phosphatase enzyme activity in human mesenchymal stem cells without osteogenic additives (article submitted). Other groups have described the secretion of anabolic bone factors by both OCl and MP extensively as well. Most recently, osteoclast-specific deletion of CTHRC1, a much sought after soluble bone coupling factor, was shown to result in osteopenia in mice emphasizing the importance of osteoclast-secreted anabolic factors on normal bone homeostasis [42]. Additionally, OCl have been reported to secrete various other osteoblast differentiating factors such as bone morphogenetic proteins (BMPs), sphingosine 1-phosphate (S1P), and Wnt10b [43–45]. Inflammatory macrophages have also been demonstrated to secrete osteogenic factors such as oncostatin M (OSM) [46,47] and may also express BMPs [48–50].

It has been suggested that macrophage-mediated inflammation may play a role in osteoinduction by CaP though until now no experiments were conducted to specifically target this cell type, nor have they shown a clear link between CaP-incited inflammation and osteoinduction [12,13]. Omar et al. (2011) did, however, show that a titanium screw coated with lipopolysaccharide (LPS) to stimulate classical activation of MP resulted in higher bone contact when in orthotopic sites [51]. On the other hand, inflammation of this sort has also been linked with osteolysis and poor osseointegration, which was ameliorated with macrophage depletion [52], suggesting long-term catabolic effects on bone rather than anabolic effects. Less clear yet is if inflammatory M1 and wound-healing M2-polarized MP may influence the bone forming capacity of biomaterials such as TCP differently. In sum, the results here substantiate the importance of MP in osteoinduction, although it is unclear if they act directly on the differentiation and bone secretion of osteoblasts or whether they mediate other cellular processes necessary for osteoinduction such as differentiating into bone-promotive OCl or secreting vasculogenic factors to increase blood flow and a supply of stem cells necessary for osteogenesis [27].

Interestingly, LipClod treatment also affected the expression of early osteoblast markers Osterix and Runx2 in TCP compared to the control, in conjunction with no bone formation and equivalent bone marker levels to non-inductive TCPb. One possible explanation for this is that macrophages and osteoclasts secrete chemotactic signals such as TNF-α, OSM, PDGF [45], and S1P that attract pre-osteoblasts. Another explanation follows the potency of macrophage- and osteoclast-secreted anabolic factors to differentiate stem cells directly. Thus, the role of these cells in osteoinduction may be to first home mesenchymal stem cells to the implant site and then differentiate them into osteoblasts by secreting anabolic trophic factors. It has been reported that osteoblast markers are up-regulated in mesenchymal stem cells cultured on similarly osteoinductive TCP [9], so the direct interaction of stem cells with an osteoinductive material may also aid osteoblast formation. However, Osterix positive cells were observed without bone formation suggesting that the activation of early osteoblast transcription factors may not guarantee bone matrix secretion of mature osteoblasts without a normally functioning phagocyte population.

Although the precise material parameters necessary for material-directed osteoinduction remain unknown, the results presented here reinforce the importance of surface microstructure and add to the growing understanding that the physical form of a biomaterial surface can invoke profoundly different tissue responses [53–56]. Here, the important role of surface microstructure was again emphasized in the disparate nature of bone formation and bone marker expression between two TCP that differ in the scale of their surface microarchitecture. By recapitulating the same bone incidence rate of these TCP as previously described in a canine intramuscular model, the FVB mouse model of subcutaneous osteoinduction recently reported by Barradas et al. (2012) was further validated. Moreover, the application of weekly LipClod injections to locally deplete invading MP at an implant surface also presents a useful strategy to evaluate the importance of the host response to different material surfaces. Indeed, the sensitivity of monocyte/macrophage-lineage cells to substrate topography alludes to an intriguing way of controlling the foreign body response by modulating the scale of surface microarchitecture.

5 Conclusion

TCP with *submicron-scale* surface architecture was found to generate TRAP positive, F4/80 negative OCl along with consistent ectopic bone formation in subcutaneous pockets of mice but TCP with *micron-scale* surface architecture did not. Liposomal Clodronate treatment, resulting in the complete depletion of TRAP positive, F4/80 negative OCl but not MP or FBGC, was found to block ectopic bone formation. Thus, the scale of TCP surface architecture may be essential to ectopic bone formation by directing the host response and subsequent osteoclastogenesis.

Acknowledgements

The authors gratefully acknowledge the support of the TeRM Smart Mix Program of the Netherlands Ministry of Economic Affairs and the Netherlands Ministry of Education, Culture and Science. This research forms part of the Project P2.04 BONE-IP of the research program of the Biomedical Materials Institute, co-funded by the Dutch Ministry of Economic Affairs. This work was also supported by funding under the Seventh Research Framework Program of the European Union, through the project REBORNE under Grant agreement no. 241879. Special thanks are due to Dr. Ana Barradas (MIRA, University of Twente) for her generous consultation with the FVB mouse model, and Jinyi Su (Xpand Biotechnology), Martine Berreur, and Jerome Amiaud (both INSERM UMR957) for their help and technical expertise.

References

[1] Arron JR, Choi Y. Bone versus immune system. Nature 2000;408:535–6.

[2] Anderson J, Rodriguez A, Chang D. Foreign Body Reaction to Biomaterials. Semin Immunol 2008;20:86–100.

[3] Mitragotri S, Lahann J. Physical approaches to biomaterial design. Nat Mater 2009;8:15–23.

[4] Magan A, Ripamonti U. Geometry of porous hydroxyapatite implants influences osteogenesis in baboons (Papio ursinus). J Craniofac Surg 1996;7:71–8.

[5] Ripamonti U, Richter PW, Nilen RWN, Renton L. The induction of bone formation by smart biphasic hydroxyapatite tricalcium phosphate biomimetic matrices in the non-human primate Papio ursinus. J Cell Mol Med 2008;12:2609–21.

[6] Habibovic P, Yuan H, van der Valk CM, Meijer G, van Blitterswijk C a, de Groot K. 3D microenvironment as essential element for osteoinduction by biomaterials. Biomaterials 2005;26:3565–75.

[7] Yuan H, De Bruijn JD, Li Y, Feng J, Yang Z, De Groot K, et al. Bone formation induced by calcium phosphate ceramics in soft tissue of dogs: a comparative study between porous alpha-TCP and beta-TCP. J Mater Sci Mater Med 2001;12:7–13.

[8] Habibovic P, Yuan H, van den Doel M, Sees TM, van Blitterswijk CA, de Groot K. Relevance of osteoinductive biomaterials in critical-sized orthotopic defect. J Orthop Res 2006;24:867–76.

[9] Yuan H, Fernandes H, Habibovic P, de Boer J, Barradas AMC, de Ruiter A, et al. Osteoinductive ceramics as a synthetic alternative to autologous bone grafting. Proc Natl Acad Sci U S A 2010;107:13614–9.

[10] Stevens MM, George JH. Exploring and engineering the cell surface interface. Science 2005;310:1135–8.

[11] Eriksson C, Nygren H, Ohlson K. Implantation of hydrophilic and hydrophobic titanium discs in rat tibia: cellular reactions on the surfaces during the first 3 weeks in bone. Biomaterials 2004;25:4759–66.

[12] Fellah BH, Josselin N, Chappard D, Weiss P, Layrolle P. Inflammatory reaction in rats muscle after implantation of biphasic calcium phosphate micro particles. J Mater Sci Mater Med 2007;18:287–94.

[13] Fellah BH, Delorme B, Sohier J, Magne D, Hardouin P, Layrolle P. Macrophage and osteoblast responses to biphasic calcium phosphate microparticles. J Biomed Mater Res A 2010;93:1588–95.

[14] Davison N, Yuan H, de Bruijn JD, Barrere-de Groot F. In vivo performance of microstructured calcium phosphate formulated in novel water-free carriers. Acta Biomater 2012;8:2759–69.

[15] Mosser DM, Edwards JP. Exploring the full spectrum of macrophage activation. Nat Rev Immunol 2008;8:958–69.

[16] Jones JA, Chang DT, Meyerson H, Colton E, Kwon IK, Matsuda T, et al. Proteomic analysis and quantification of cytokines and chemokines from biomaterial surface-adherent macrophages and foreign body giant cells. J Biomed Mater Res A 2007;83:585–96.

[17] Takayanagi H. Osteoimmunology: shared mechanisms and crosstalk between the immune and bone systems. Nat Rev Immunol 2007;7:292–304.

[18] Sima C, Glogauer M. Macrophage subsets and osteoimmunology: tuning of the immunological recognition and effector systems that maintain alveolar bone. Periodontol 2000 2013;63:80–101.

[19] Steeve KT, Marc P, Sandrine T, Dominique H, Yannick F. IL-6, RANKL, TNF-alpha/IL-1: interrelations in bone resorption pathophysiology. Cytokine Growth Factor Rev 2004;15:49–60.

[20] Theoleyre S, Wittrant Y, Tat SK, Fortun Y, Redini F, Heymann D. The molecular triad OPG/RANK/RANKL: involvement in the orchestration of pathophysiological bone remodeling. Cytokine Growth Factor Rev 2004;15:457–75.

[21] Stein NC, Kreutzmann C, Zimmermann S-P, Niebergall U, Hellmeyer L, Goettsch C, et al. Interleukin-4 and interleukin-13 stimulate the osteoclast inhibitor osteoprotegerin by human endothelial cells through the STAT6 pathway. J Bone Miner Res 2008;23:750–8.

[22] Kondo N, Ogose A, Tokunaga K, Umezu H, Arai K, Kudo N, et al. Osteoinduction with highly purified beta-tricalcium phosphate in dog dorsal muscles and the proliferation of osteoclasts before heterotopic bone formation. Biomaterials 2006;27:4419–27.

[23] Tanaka T, Saito M, Chazono M, Kumagae Y, Kikuchi T, Kitasato S, et al. Effects of alendronate on bone formation and osteoclastic resorption after implantation of beta-tricalcium phosphate. J Biomed Mater Res A 2010;93:469–74.

[24] Ripamonti U, Klar RM, Renton LF, Ferretti C. Synergistic induction of bone formation by hOP-1, hTGF-beta3 and inhibition by zoledronate in macroporous coral-derived hydroxyapatites. Biomaterials 2010;31:6400–10.

[25] Kan L, Liu Y, McGuire TL, Berger DMP, Awatramani RB, Dymecki SM, et al. Dysregulation of local stem/progenitor cells as a common cellular mechanism for heterotopic ossification. Stem Cells 2009;27:150–6.

[26] Alexander K a, Chang MK, Maylin ER, Kohler T, Müller R, Wu AC, et al. Osteal macrophages promote in vivo intramembranous bone healing in a mouse tibial injury model. J Bone Miner Res 2011;26:1517–32.

[27] Glass GE, Chan JK, Freidin A, Feldmann M, Horwood NJ, Nanchahal J. TNF-alpha promotes fracture repair by augmenting the recruitment and differentiation of muscle-derived stromal cells. Proc Natl Acad Sci U S A 2011;108:1585–90.

[28] Barradas AMC, Yuan H, van der Stok J, Le Quang B, Fernandes H, Chaterjea A, et al. The influence of genetic factors on the osteoinductive potential of calcium phosphate ceramics in mice. Biomaterials 2012;33:5696–705.

[29] Van Rooijen N, van Kesteren-Hendrikx E. "In vivo" depletion of macrophages by liposome-mediated "suicide". Methods Enzymol 2003;373:3–16.

[30] Takahashi N, Udagawa N, Tanaka S, Murakami H, Owan I, Tamura T, et al. Postmitotic osteoclast precursors are mononuclear cells which express macrophage-associated phenotypes. Dev Biol 1994;163:212–21.

[31] Hume DA, Loutit JF, Gordon S. The mononuclear phagocyte system of the mouse defined by immunohistochemical localization of antigen F4/80: macrophages of bone and associated connective tissue. J Cell Sci 1984;66:189–94.

[32] Boyle W, Simonet W, Lacey D. Osteoclast differentiation and activation. Nature 2003;423:337–42.

[33] Wenisch S, Stahl J-P, Horas U, Heiss C, Kilian O, Trinkaus K, et al. In vivo mechanisms of hydroxyapatite ceramic degradation by osteoclasts: fine structural microscopy. J Biomed Mater Res A 2003;67:713–8.

[34] Dersot JM, Colombier ML, Lafont J, Baroukh B, Septier D, Saffar JL. Multinucleated giant cells elicited around hydroxyapatite particles implanted in craniotomy defects are not osteoclasts. Anat Rec 1995;242:166–76.

[35] Baslé MF, Chappard D, Grizon F, Filmon R, Delecrin J, Daculsi G, et al. Osteoclastic resorption of Ca-P biomaterials implanted in rabbit bone. Calcif Tissue Int 1993;53:348–56.

[36] Eggli PS, Müller W, Schenk RK. Porous hydroxyapatite and tricalcium phosphate cylinders with two different pore size ranges implanted in the cancellous bone of rabbits. A comparative histomorphometric and histologic study of bony ingrowth and implant substitution. Clin Orthop Relat Res 1988:127–38.

[37] Van Rooijen N. The liposome-mediated macrophage “suicide” technique. J Immunol Methods 1989;124:1–6.

[38] Metabolite A, Ylitalo K V, Mönkkönen J, Rogers MJ, Azhayev A, Kalervo HVA, et al. Further Insight into Mechanism of Action of Clodronate□ : Inhibition of Mitochondrial ADP / ATP Translocase by a. Med Biochem 2002;62:1255–62.

[39] Frith JC, Mönkkönen J, Blackburn GM, Russell RG, Rogers MJ. Clodronate and liposome-encapsulated clodronate are metabolized to a toxic ATP analog, adenosine 5’-(beta, gamma-dichloromethylene) triphosphate, by mammalian cells in vitro. J Bone Miner Res 1997;12:1358–67.

[40] Wang W, Ferguson DJ, Quinn JM, Simpson AH, Athanasou NA. Osteoclasts are capable of particle phagocytosis and bone resorption. J Pathol 1997;182:92–8.

[41] Frith JC, Mönkkönen J, Auriola S, Mönkkönen H, Rogers MJ. The molecular mechanism of action of the antiresorptive and antiinflammatory drug clodronate: evidence for the formation in vivo of a metabolite that inhibits bone resorption and causes osteoclast and macrophage apoptosis. Arthritis Rheum 2001;44:2201–10.

[42] Takeshita S, Fumoto T, Matsuoka K, Park K, Aburatani H, Kato S, et al. Osteoclast-secreted CTHRC1 in the coupling of bone resorption to formation. J Clin Invest 2013;123:3914–24.

[43] McCullough KA, Waits CA, Garimella R, Tague SE, Sipe JB, Anderson HC. Immunohistochemical localization of bone morphogenetic proteins (BMPs) 2, 4, 6, and 7 during induced heterotopic bone formation. J Orthop Res 2007;25:465–72.

[44] Pederson L, Ruan M, Westendorf JJ, Khosla S, Oursler MJ. Regulation of bone formation by osteoclasts involves Wnt/BMP signaling and the chemokine sphingosine-1-phosphate. Proc Natl Acad Sci U S A 2008;105:20764–9.

[45] Kreja L, Brenner RE, Tautzenberger A, Liedert A, Friemert B, Ehrnthaller C, et al. Non-resorbing osteoclasts induce migration and osteogenic differentiation of mesenchymal stem cells. J Cell Biochem 2010;109:347–55.

[46] Guihard P, Danger Y, Brounais B, David E, Brion R, Delecrin J, et al. Induction of osteogenesis in mesenchymal stem cells by activated monocytes/macrophages depends on oncostatin m signaling. Stem Cells 2012;30:762–72.

[47] Nicolaidou V, Wong MM, Redpath AN, Ersek A, Baban DF, Williams LM, et al. Monocytes induce STAT3 activation in human mesenchymal stem cells to promote osteoblast formation. PLoS One 2012;7(7): e398:e39871.

[48] Champagne CM, Takebe J, Offenbacher S, Cooper LF. Macrophage cell lines produce osteoinductive signals that include bone morphogenetic protein-2. Bone 2002;30:26–31.

[49] Honda Y, Anada T, Kamakura S, Nakamura M, Sugawara S, Suzuki O. Elevated extracellular calcium stimulates secretion of bone morphogenetic protein 2 by a macrophage cell line. Biochem Biophys Res Commun 2006;345:1155–60.

[50] Takebe J, Champagne CM, Offenbacher S, Ishibashi K, Cooper LF. Titanium surface topography alters cell shape and modulates bone morphogenetic protein 2 expression in the J774A.1 macrophage cell line. J Biomed Mater Res A 2003;64:207–16.

[51] Omar OM, Granéli C, Ekström K, Karlsson C, Johansson A, Lausmaa J, et al. The stimulation of an osteogenic response by classical monocyte activation. Biomaterials 2011;32:8190–204.

[52] Ren W, Markel DC, Schwendener R, Ding Y, Wu B, Wooley PH. Macrophage depletion diminishes implant-wear-induced inflammatory osteolysis in a mouse model. J Biomed Mater Res A 2008;85:1043–51.

[53] Chen S, Jones J a, Xu Y, Low H-Y, Anderson JM, Leong KW. Characterization of topographical effects on macrophage behavior in a foreign body response model. Biomaterials 2010;31:3479–91.

[54] Zhang W, Wang G, Liu Y, Zhao X, Zou D, Zhu C, et al. Biomaterials The synergistic effect of hierarchical micro / nano-topography and bioactive ions for enhanced osseointegration. Biomaterials 2013;34:3184–95.

[55] Jäger M, Zilkens C, Zanger K, Krauspe R. Significance of Nano- and Microtopography for Cell-Surface Interactions in Orthopaedic Implants. J Biomed Biotechnol 2007;2007:1–19.

[56] Thomsen P, Gretzer C. Macrophage interactions with modified material surfaces. Curr Opin Solid State Mater Sci 2001;5:163–76.

Figure 1. Ectopic bone formation by TCPs and blockade by phagocyte depletion. (Top) Representative sections stained with Masson's Trichrome from decalcified TCP (black stars) cubes subcutaneously implanted in mice for 12 weeks. Ectopic bone formation (white stars) was only found in TCPs (A, B), shown by dark green collagen staining. Osteocytes in lacunae (A, open arrows) and cuboidal osteoblasts (B, black arrows) can be seen in and on the mature bone matrix. Local liposomal clodronate injections blocked bone formation in TCPs (TCPs + LipClod) (C, D). Connective tissue in the pore space was generally less condensed (C, light green) though blood vessels were still formed (D, orange stained erythrocytes). TCPb (E, F) formed no bone although the pore structure was vascularized (E, orange erythrocytes) and cells had colonized the material surface (F, grey staining). 10x scale bar = 4 mm; 40x scale bar = 100 µm. (Bottom) Gene expression of mature bone markers osteocalcin and bone sialoprotein were up-regulated in TCPs versus TCPs + LipClod and TCPb, while expression levels between TCPs + LipClod and non-inductive TCPb were equivalent. * $P < 0.05$, ** $P < 0.01$, *** $P < 0.001$.

Figure 2. Osteoclastogenesis by TCPs and depletion by Liposomal Clodronate. (Top) Representative overview images (10x) stained with Masson's Trichrome show ectopic bone formation in TCPs (dark green) and not in TCPs treated with Liposomal Clodronate (LipClod) or non-inductive TCPb. (A, B) 40x insets of serial sections stained for osteoclast marker tartrate resistant acid phosphatase (TRAP) and macrophage membrane marker F4/80 show TRAP positive (red) F4/80 negative osteoclasts colonizing the material (black stars) between stretches of ectopic bone (white stars). No TRAP positive cells could be found in TCPs treated with Liposomal Clodronate (LipClod) (C, D) or the non-inductive TCPb (E, F). Multinucleated cells (black arrows) in these explants were uniformly F4/80 positive (brown) fused macrophages. 10x scale bar = 200 µm; 40x scale bar = 100 µm. (Bottom) Gene expression of osteoclast markers TRAP, CTR, and NFATc1 were significantly upregulated in TCPs versus TCPs + LipClod or TCPb. Expression of RANK was down-regulated in TCPs + LipClod versus TCPs, indicative of pre-osteoclast depletion. Expression levels of RANKL and its decoy receptor OPG varied between groups but were statistically equivalent. * $P < 0.05$, ** $P < 0.01$.

Figure 3. Macrophage colonization of TCP and depletion by Liposomal Clodronate. (Top) Representative sections of TCP (black stars) immunohistochemically stained for macrophage membrane marker F4/80. F4/80 positive macrophages (brown) densely lined the (A) outer surface and (B) inner pore structure of TCPs, resembling osteal macrophages. Weekly liposomal Clodronate injections (TCPs + LipClod) effectively depleted F4/80 positivity at the (C) outer surface of TCPs with evident cell fragments indicative of apoptosis due to the treatment; however F4/80 positive macrophages still colonized the (D) inner pore structure. Positively stained macrophages less densely colonized the (E) outer surface and (F) inner pore structure of TCPb (TCP marked by black stars). 5x scale bar = 1 mm; 20x scale bar = 300 µm. (Bottom) Gene expression of F4/80 was equivalent between all groups.

Figure 4. Osteoblast differentiation by TCPs is inhibited by phagocyte depletion.

(Top) Immunohistochemical staining of osteoblast marker Osterix in (left) Osterix positive cells (black arrows) were found colonizing the surface of TCPs (black stars) as well as bone tissue (white stars) containing osteocytes in lacunae (open arrows). (Right) Positively stained cells were also found in TCPs treated with Liposomal Clodronate (TCPs + LipClod) but to a lesser extent, both in the (top) inter-pore space and (bottom) in contact with the TCP surface, despite no bone formation. (Bottom) Gene expression of Runx2 was up-regulated in TCPs versus TCPs + LipClod, which was at an equivalent level as non-inductive TCPb. * $P < 0.05$.

Table 1. Physical characterization of TCP

Physical parameters	TCPs	TCPb
Average grain diameter	0.95 ± 0.27	3.66 ± 1.05
Average pore diameter	0.63 ± 0.33	1.78 ± 0.85
Average peak-to-valley roughness, R_a	0.126 ± 0.003	1.287 ± 0.011
Root-mean-square peak-to-valley roughness, R_{RMS}	0.158 ± 0.003	1.597 ± 0.011
Porosity (%)	69.6	72.0
Total pore area (m^2/g)	1.477	0.769

Table 2. qPCR primer sequences

Gene Target	Sequence (5' -> 3')	Product size (bp)	Accession ID
HPRT	tcctcctcagaccgctttt cctggttcatcatcgctaatc	90	NM_013556.2
Cyc1	tgtgctacacggaggaagaa catcatcattagggccatcc	72	NM_025567.1
RANKL	tcctgtactttcgagcgcag ttatgggaacccgatgggatg	337	NM_011613.3
CTK	ggaggcggctatatgacca ggcgttatacatacaactttcatcc	111	NM_007802.4
TRAP	cgtctctgcacagattgcat aagcgcaaacggtagtaagg	75	NM_001102405.1
CTR	ccttccagaggagaagaaacc ggagattccgccttttcac	95	NM_007588.2
OC	agactccggcgctacctt caagcagggttaagctcaca	86	NM_001032298.2
RANK	tgcagctcttccatgacactg cagccactactaccacagagatg	103	NM_009399.3
OPG	atgaacaagtggctgtgctg cagtttctgggtcataatgcaa	106	NM_008764.3
Runx2	ccacaaggacagagtcagattaca tggctcagataggaggggta	92	NM_001145920.2
F4/80	tcctccttgcctggacact gccttgaaggtcagcaacc	100	NM_010130.4
NFATc1	catgcgagccatcatcga tgggatgtgaactcggaagac	130	NM_001164112.1

Table 3. Incidence rate of ectopic bone formation by histological analysis.

TCPs	TCPs + LipClod	TCPb
7/7	0/5	0/8

Figure 1
Click here to download high resolution image

Fig. 1

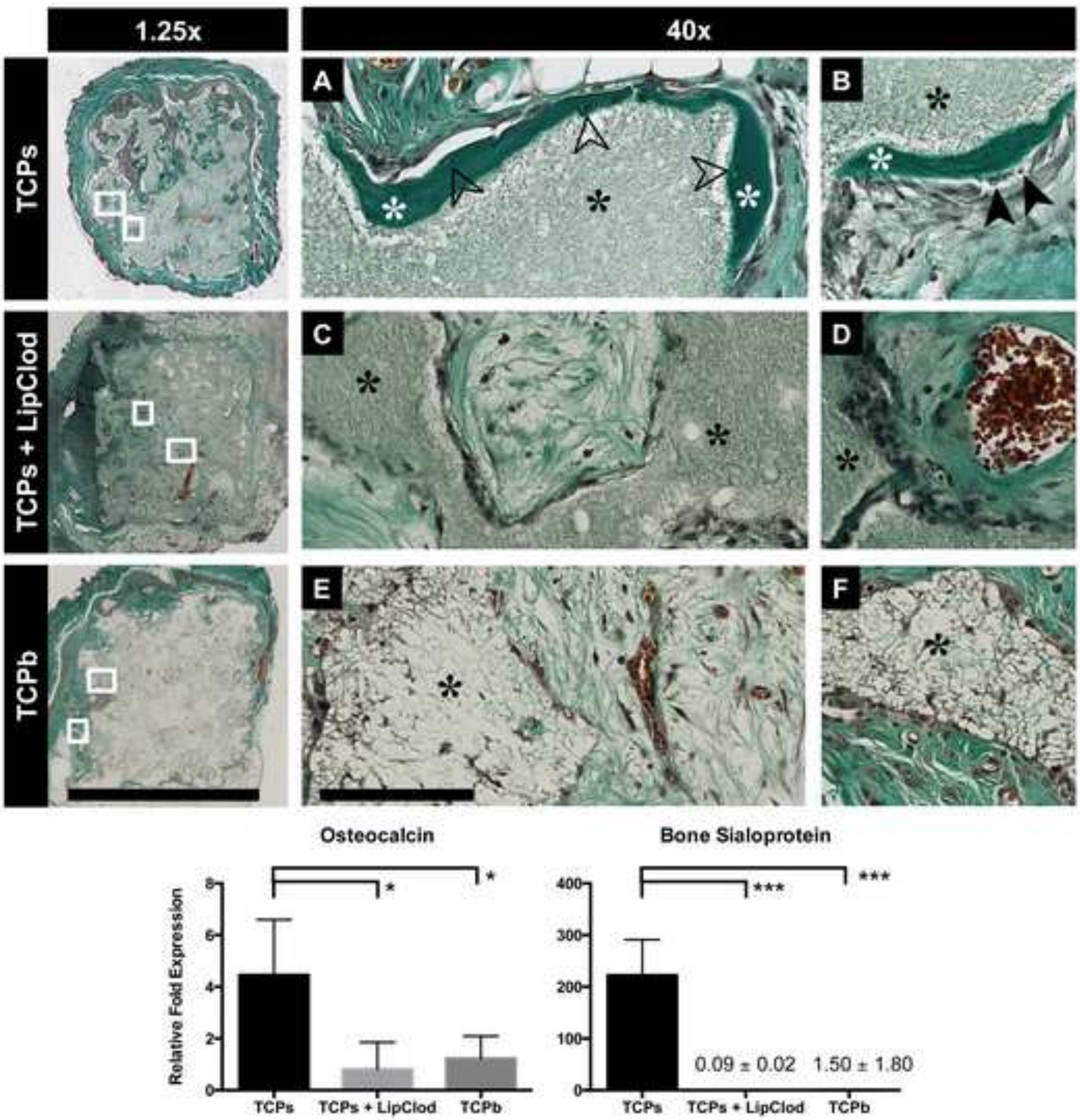

Figure 2
Click here to download high resolution image

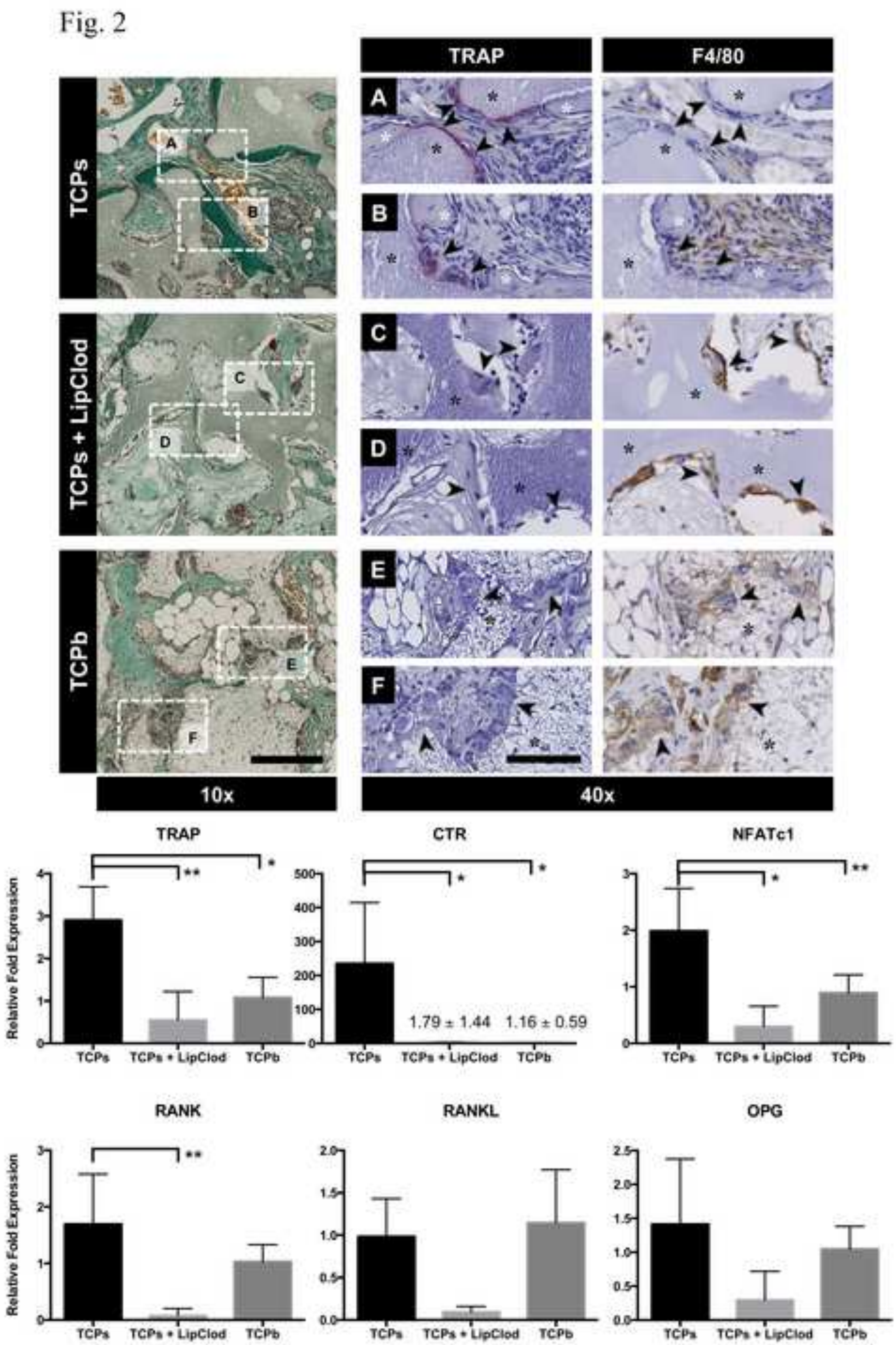

Figure 3
Click here to download high resolution image

Fig. 3

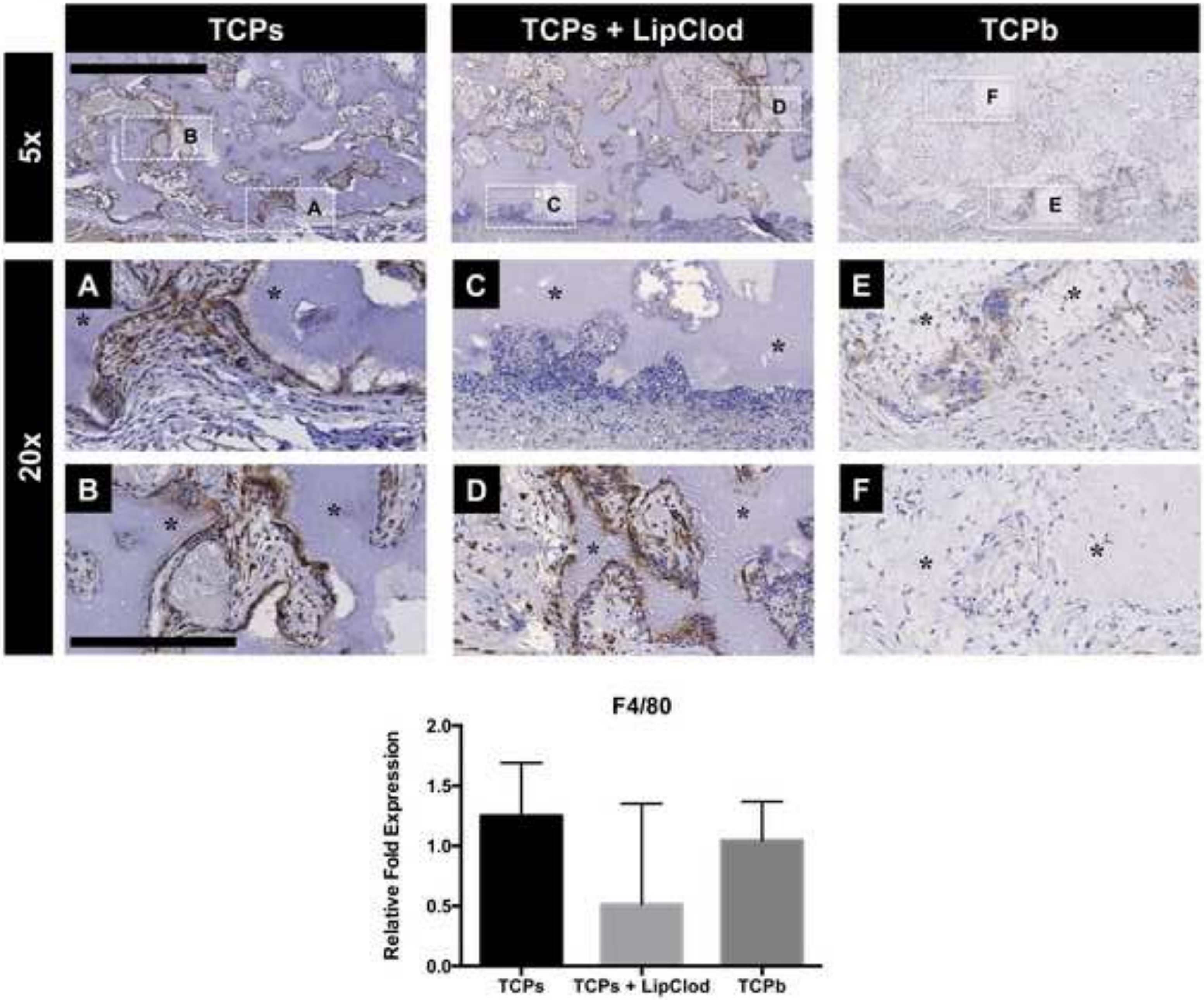

Figure 4
Click here to download high resolution image

Fig 4